Progress In Electromagnetics Research, PIER 104, 1–13, 2010

UWB CIRCULAR SLOT ANTENNA PROVIDED WITH AN INVERTED-L NOTCH FILTER FOR THE 5 GHz WLAN BAND

S. Barbarino †

Dipartimento di Fisica e Astronomia
Università degli Studi di Catania
Via S. Sofia 64, 95123 Catania, Italy

F. Consoli

Laboratori Nazionali del Sud
Istituto Nazionale di Fisica Nucleare
Via S. Sofia 62, 95123 Catania, Italy

Abstract—The study of a planar circular slot antenna for Ultrawideband (UWB) communications is presented. The integration on this antenna of a notch filter, to reduce the possible interferences with the 5 GHz WLAN communications, has been discussed in detail. Four different structures, achieved by etching a suitable pattern on the antenna circular stub, have been considered, and their features have been compared. The antenna with symmetrical and inverted-L cuts shows the best performance, and it has been therefore realized and fully characterized. It shows very good matching features over the UWB band, and notable rejection of the 5 GHz WLAN band.

1. INTRODUCTION

In this paper, we discuss the study of an Ultrawideband (UWB) [1, 2] planar circular slot antenna, having $R = 10$ mm slot radius. In order to fulfil the UWB bandwidth requirements, we used a 50 Ω microstrip feed, ending with a circular stub [3], and in the optimization process we considered all the antenna parameters, for fixed slot radius. The scheme of this structure, named *Antenna X*, is shown in Figure 1.

Corresponding author: F. Consoli (consoli@lns.infn.it).
† Also with Dipartimento di Ingegneria Informatica e delle Telecomunicazioni, Università degli Studi di Catania, Viale A. Doria 6, 95125 Catania, Italy.

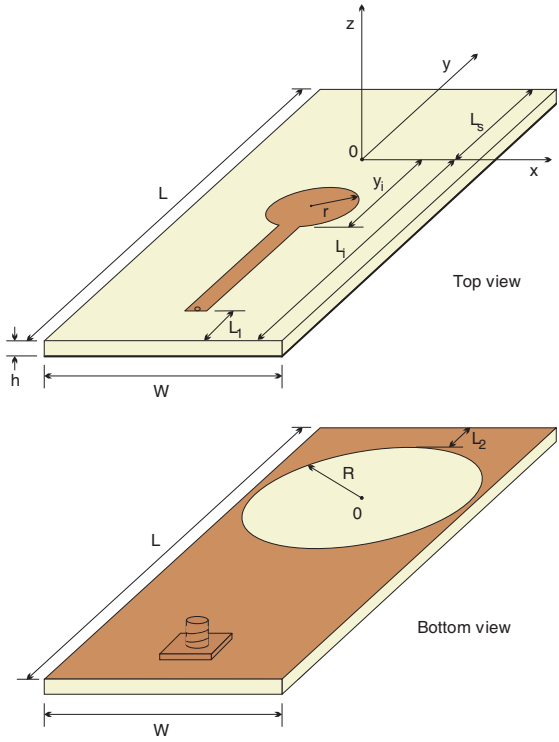

Figure 1. Top view and bottom view of the *Antenna X* layout.

Subsequently, a filter has been added to the antenna, to reject the 5 GHz WLAN band [1, 2].

2. ANTENNA DESCRIPTION AND STUDY

The antenna substrate is the RT/duroid 5870, having $\epsilon_r = 2.33$ and $h = 1.575\,\text{mm}$ thickness. A substrate with such low electric permittivity has been used in order to favour the antenna wideband features, and to have radiation properties more stable with respect to the frequency [4]. Accurate time domain electromagnetic simulations, performed by means of CST Microwave Studio solver, have been accomplished for the optimization process. The reflection coefficient of the resulting *Antenna X*, supplied by a suitable Fourier transformation, is shown in Figure 2, while in Table 1 the values for all of its parameters are given. The values of $f_{\min}$ and $f_{\max}$, extremes of the matched band (for a $VSWR \leq 2$), are also supplied. The antenna impedance bandwidth is (3.012, 14.374) GHz.

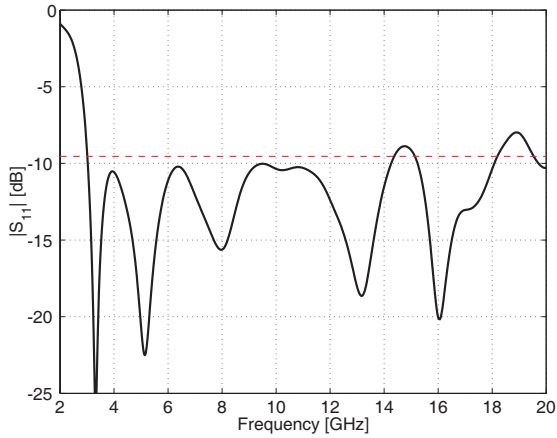

Figure 2. Simulation of the reflection coefficient for the antenna with circular stub (*Antenna X*).

Table 1. Parameters of the optimized structures. X: antenna with circular stub; A: antenna with symmetrical and inverted-L cuts; B: antenna with low circular cut; C: antenna with high circular cut; D: antenna with H-type cut.

	X	A	B	C	D
W [mm]	20.1	20.4	20.1	20.1	20.4
L_i [mm]	45	48	44.5	44	48
L_s [mm]	16	16	16	16.7	16
y_i [mm]	10.4	10.4	10.5	10.4	10.6
r [mm]	7	7.2	6.6	6.6	6.8
L_1 [mm]	6	9	6	6	9
L_2 [mm]	6	6	6	6.7	6
s_1 [mm]		6	3	1.5	0.7
s_2 [mm]		3.1	4.7	5.1	6.2
s_3		7 mm	110°	145°	10.5 mm
s_4 [mm]		0.7	0.2	0.6	0.2
$f_{\min}$ [GHz]	3.012	3.019	3.089	3.101	3.101
$f_{\max}$ [GHz]	14.374	18.716	14.911	14.904	14.704
f_{n_1} [GHz]		4.912	4.996	4.956	4.794
f_{n_2} [GHz]		6.289	7.295	7.110	7.400

In order to improve the use of this antenna for the UWB communications, the integration of a notch filter on this structure has been studied in detail. It is needed to minimize the potential interference with the WLAN communications in the $(5.150, 5.825)$ GHz band $[1, 2]$. Among all the various proposals, we have focused our attention on filters achieved by etching a suitable pattern on the antenna stub. In particular, we considered the application of two *symmetrical and inverted-L* cuts [5], a *low circular* cut [6], a *high circular* cut [7], and an *H-type* cut [8] to the circular stub. The comparison between the performances produced by etchings with these shapes, when they are applied to this circular slot antenna fed by a microstrip ending with a circular stub, is described here. The choice of these simple patterns, from all the types present in literature, has been carried out to have high filter performances, together with a small number of degrees of freedom. They are illustrated in Figure 3. For each of these layouts, the optimization process has taken into account again all the antenna parameters, for fixed slot radius. The reflection coefficient of the optimized structures is compared in Figure 4, whereas all of their parameters are given in Table 1. The f_{n1} and f_{n2} extremes of the notched band are also supplied. The observation of Figure 4 shows that, despite their simple shape, all the considered etchings allow the achievement of a high mismatching in the 5 GHz band. Moreover, they have a large impedance bandwidth (for a $VSWR \leq 2$), fulfilling the UWB requirements. The antenna with symmetrical inverted-L cuts (*Antenna A*), has the most selective notched band, the largest matched band and also the best impedance matching within

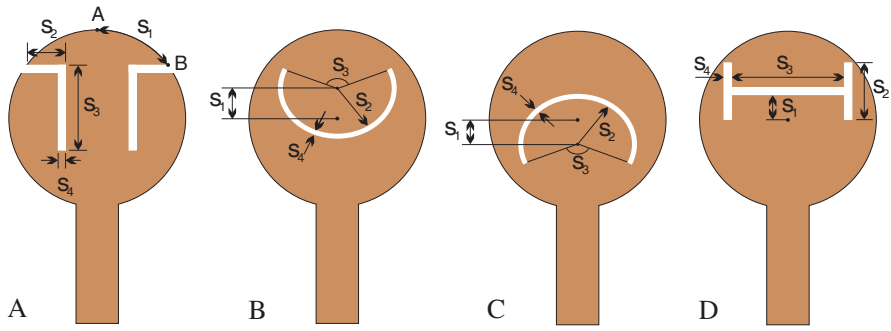

Figure 3. Different considered patch etchings for the filter realization. A: patch with two symmetrical and inverted-L cuts; B: patch with circular cut directed downwards (*low circular*); C: patch with circular cut directed upwards (*high circular*); D: patch with H shaped cut.

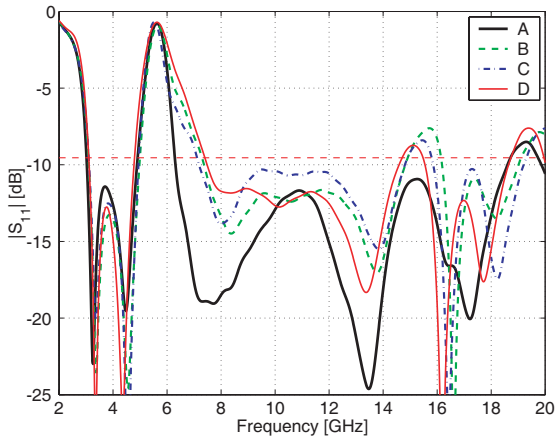

Figure 4. Comparison among the simulated $|S_{11}|$ of the antennas having patch shapes described in Figure 3, and parameters given in Table 1.

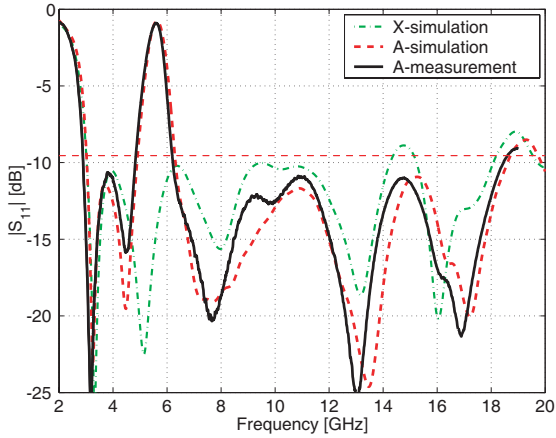

Figure 5. Comparison among the $|S_{11}|$ of *Antenna X* and *Antenna A*.

this band. This has been therefore realized and fully experimentally characterized. In Figure 5, the measured $|S_{11}|$ of this prototype has been compared with the simulation results for the same structure and for the original *Antenna X*. A very good agreement between results achieved by simulations and by measurements is observed. The notable bandwidth increasing, and the improvement of the general impedance matching over the UWB band, are observed for the realized antenna with respect to *Antenna X*.

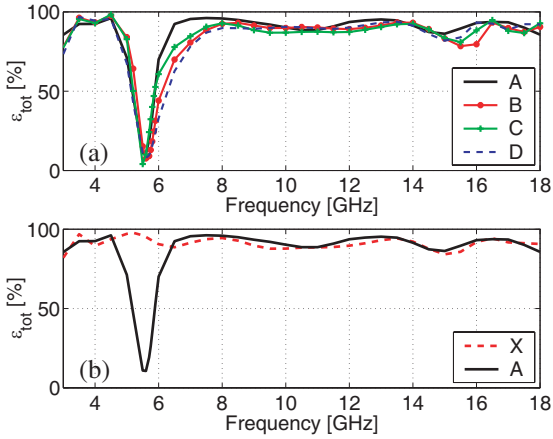

Figure 6. (a) Comparison among the ϵ_{tot} of the antennas having patch shapes described in Figure 3, and parameters given in Table 1. (b) Comparison among the ϵ_{tot} of *Antenna X* and *Antenna A*.

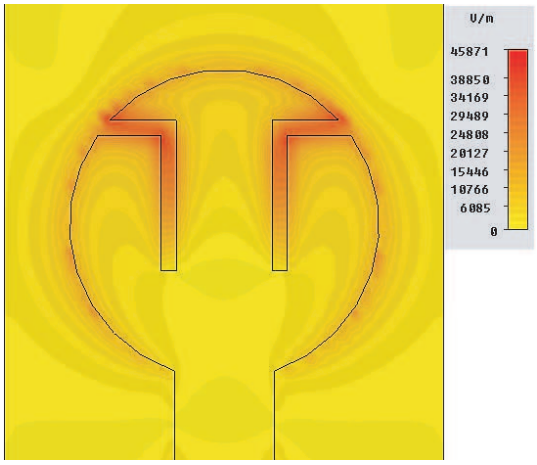

Figure 7. Simulated electric field distribution at $f = 5.5$ GHz for the *Antenna A* stub.

The evaluation of the $\epsilon_{tot} = (1 - |S_{11}|^2)\ \epsilon_{rad}$ total efficiency [9], which takes into account both the ϵ_{rad} radiation efficiency and the impedance matching, has also been performed for all the analyzed structures. In particular, Figure 6(a) shows the comparison among the total efficiencies for all the optimized structures with integrated filters illustrated in Figure 3. A high rejection (with $\epsilon_{tot} \approx 10\%$) is

observed within the 5 GHz band, whereas an average $\epsilon_{tot} \approx 90\%$ is achieved outside of it. The *Antenna A*, with the inverted-L filter, shows the best behaviour in terms of selectivity for the notched band and of efficiency outside of it. In Figure 6(b), the efficiencies of this antenna and of *Antenna X* are compared. A small improvement for the ϵ_{tot} of *Antenna A* is observed. The electromagnetic study of each of these structures has also shown that within the 5 GHz rejected band the electromagnetic field is mainly distributed in the etched region of the circular stub. This is represented in Figure 7, where the simulated electric field profile for $f = 5.5$ GHz is shown for *Antenna A*. This causes the inhibition of the antenna radiation properties. In this work, it is shown how the etching shape is a factor that can be useful to properly tune the characteristics of this behaviour.

Radiation and time domain features of the optimized *Antenna A* are described below. In Figure 8, the results of simulations and measurements for the normalized antenna gain are shown for $f = 4$ GHz and $f = 8$ GHz frequencies. The G_ϕ component on the yz plane is not given for symmetry reasons. The differences, between the measured radiation patterns (more evident for the G_ϕ component on the xz plane, at 4 GHz) and the simulations, are due to the influence of the measurement set-up on the antenna radiation properties, and to the antenna fabrication tolerances. In Figure 9, the tridimensional views of the simulated antenna absolute gain are shown for different frequencies. The observation of this figure shows that more lobes are present for larger frequencies.

In Figure 10, the absolute gain is given along the $\theta = 0^\circ$ and $\theta = 180^\circ$ directions. Results for both simulations and measurements are supplied along the (3, 18) GHz band. The gain displays large variations with respect to the frequency. The effect of the filter for the 5 GHz band is evident.

The antenna radiation properties at the different frequencies can be described also by the $TF(\omega)$ transmission function between the wave at the antenna input and the radiated electric field along the $\theta = 0^\circ$ direction, at a 1.5 m distance. This is determined by electromagnetic simulations; for each frequency the radiated electric field, relative to a 1 W monochromatic wave feeding the antenna [10], is calculated. The associated *group delay* of the radiated electric field can be calculated as [11]:

$$t_g = -\frac{d}{d\omega}\left[\angle\, TF(\omega)\right]. \tag{1}$$

In Figure 11, the comparison of the $|TF|$ and the t_g amounts, for *Antenna X* and *Antenna A*, is shown. A significative perturbation for both parameters, due to the presence of the filter, is observed

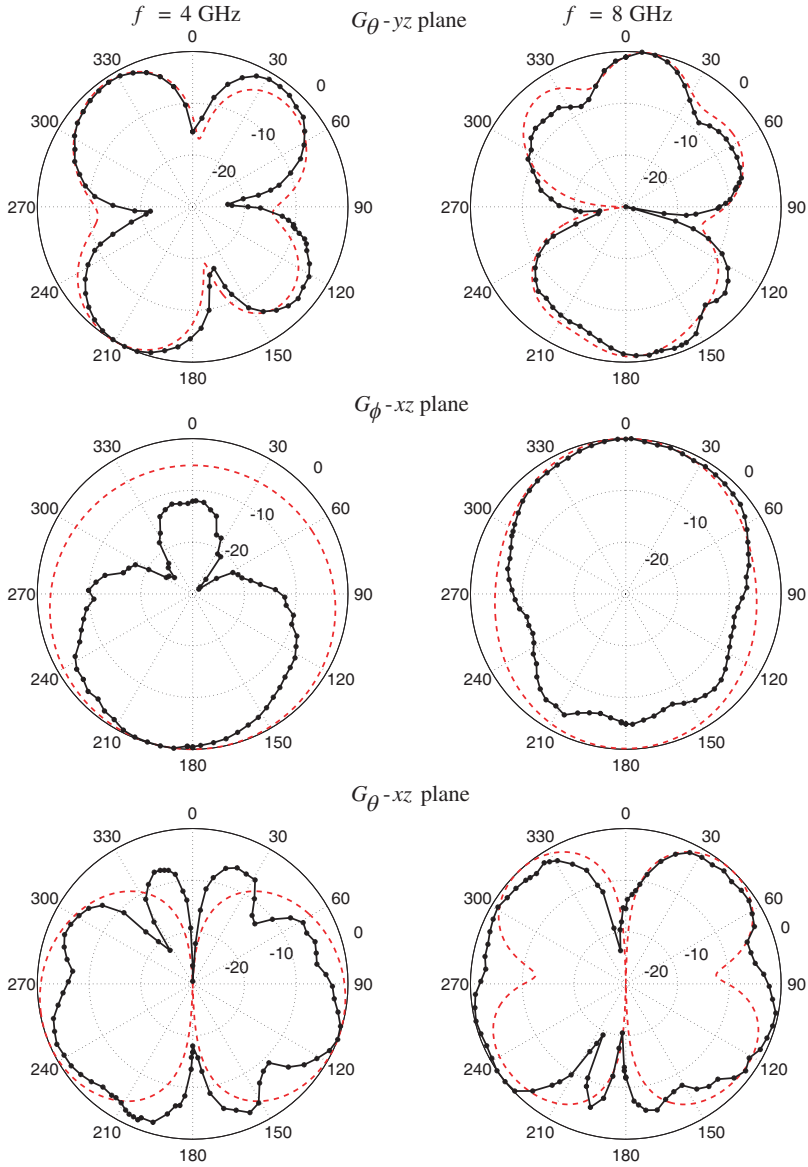

Figure 8. Simulations (red dashed line) and measurements (black marked line) of the normalized gain components of *Antenna A*, expressed in dB, on the yz and xz planes, for the $f = 4\,\text{GHz}$ and $f = 8\,\text{GHz}$ frequencies.

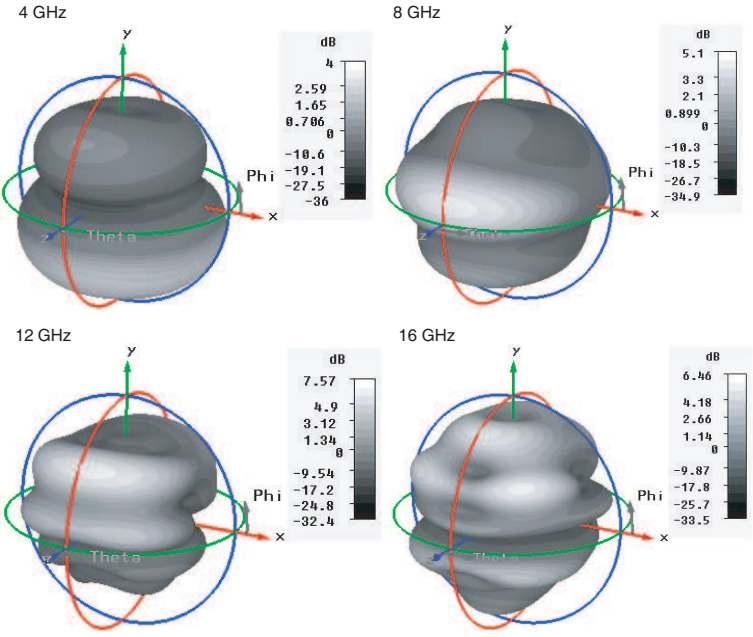

Figure 9. Simulations of the antenna tridimensional absolute gain for different frequencies.

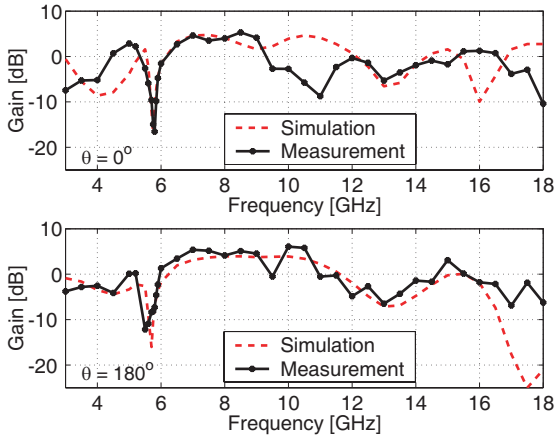

Figure 10. Simulations and measurements of the absolute gain for *Antenna A*, on the $\theta = 0^\circ$ and $\theta = 180^\circ$ directions.

around the $f = 5.8\,\mathrm{GHz}$ frequency, whereas they almost coincide with those of *Antenna X*, away from it. While $|TF|$ is notably changing with frequency, an almost constant $t_g \approx 5.4\,\mathrm{ns}$ is observed. In Figure 12, the time evolution of the radiated electric field, for $\theta = 0°$ and $z = 1.5\,\mathrm{m}$, is shown for these two antennas, when the signal at

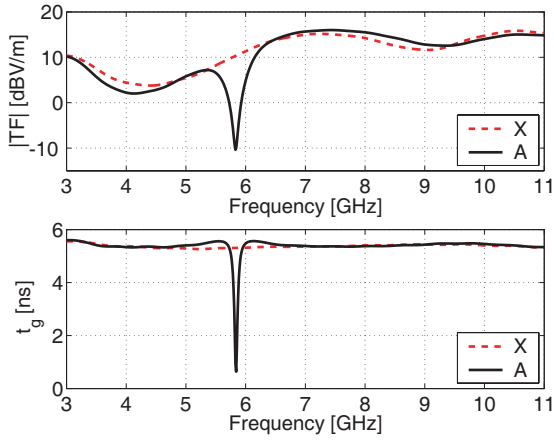

Figure 11. $|TF|$ and t_g for *Antenna X* and *Antenna A*, along the $\theta = 0°$ direction and for $z = 1.5$ m.

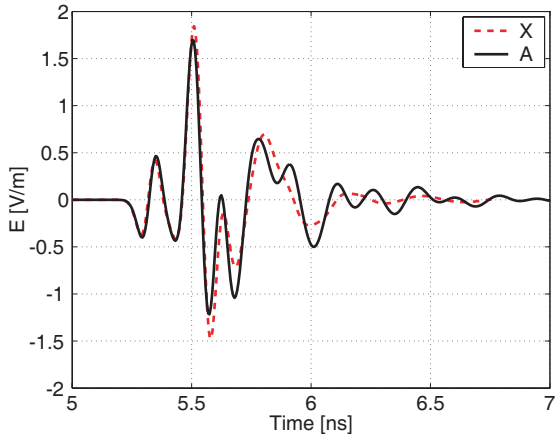

Figure 12. $E(t)$ for $\theta = 0°$ and $z = 1.5\,\mathrm{m}$, when the gaussian pulse of Formula (2) is at the inputs of *Antenna X* and *Antenna A*.

their inputs is a normalized time-shifted gaussian pulse:

$$G(t) = k\, e^{\frac{(t-\mu)^2}{2\sigma^2}} \tag{2}$$

where k is a constant, $\mu = 161.5\,\text{ps}$ and $\sigma = 31\,\text{ps}$, which has a frequency content covering the UWB range [10]. Despite the perturbations shown in Figure 11, no remarkable differences appear to be produced in the antenna time domain feature by the filter integration. In order to quantify these differences, for any θ and ϕ direction, it is possible to estimate the *Fidelity* (F) [2, 11, 16]:

$$F(x,y) = \max_{\tau} \left| \frac{\int_{-\infty}^{+\infty} x(t,\theta,\phi) \cdot y(t-\tau,\theta,\phi)dt}{\sqrt{\int_{-\infty}^{+\infty} |x(t,\theta,\phi)|^2} \cdot \sqrt{\int_{-\infty}^{+\infty} |y(t,\theta,\phi)|^2 dt}} \right| \tag{3}$$

between the radiated electric field components of *Antenna X* and *Antenna A* at 1.5 m distance. In particular, because of the antenna symmetry with respect to the yz plane, only the θ component of the electric field has been considered on this plane. The calculations give $F = 93.10\%$ for $\theta = 0°$ (which regards the plots shown in Figure 12) and $F = 94.59\%$ for $\theta = 180°$. In Table 2, the calculated F, for both θ and ϕ components, and along different θ and ϕ directions, is supplied. High values are achieved for F along all the considered directions. These calculations confirms that the filter integration within this slot antenna produces very small perturbations on the time evolution of the radiated fields.

Table 2. Calculated percentage *Fidelity* (F) between the components of the radiated electric fields of *Antenna X* and *Antenna* A, at 1.5 m distance, for different θ and ϕ directions.

	$F(E_{\theta X}, E_{\theta A})$ $\phi = 0°$	$F(E_{\phi X}, E_{\phi A})$ $\phi = 0°$	$F(E_{\theta X}, E_{\theta A})$ $\phi = 90°$	$F(E_{\theta X}, E_{\theta A})$ $\phi = 270°$
$\theta = 30^o$	95.86 %	93.10 %	86.95 %	92.00%
$\theta = 60^o$	95.52 %	92.89 %	96.59 %	85.74%
$\theta = 90^o$	97.42 %	92.67 %	95.36 %	90.07%
$\theta = 120^o$	98.34 %	93.38 %	96.29 %	90.37%
$\theta = 150^o$	96.40 %	94.25 %	88.14 %	93.34%

3. CONCLUSION

This study has produced a compact planar slot antenna, having 20.4 mm width and 64 mm length, integrated with an inverted-L filter.

The measurements show that the realized prototype is matched in the $(2.883, 18.604)$ GHz band, with a $(4.844, 6.190)$ GHz rejection band (i.e., where $VSWR > 2$). In particular, a high maximum value of 19.3 has been reached for the $VSWR$, with a minimum value of 4.2, over the $(5.150, 5.825)$ GHz WLAN band. This antenna is therefore suitable for application in the UWB communications, and presents large reduction of the possible interferences with the 5 GHz WLAN communications. The comparison with other antennas, available in literature, for the same application and having smaller dimensions [6, 12–15], shows that this prototype has a simpler structure and a smaller number of degrees of freedom, presents much higher rejection to the possible interference with the 5 GHz WLAN communications, and has larger matched band.

REFERENCES

1. Schantz, H., *The Art and Science of Ultrawideband Antennas*, Artech House, Norwood, 2005.
2. Arslan, H., Z. N. Chen, and M.-G. Di Benedetto, *Ultra-wideband Wireless Communication*, John Wiley and Sons, Hoboken, 2006.
3. Denidni, T. A. and M. A. Habib, "Broadband printed CPW-fed circular slot antenna," *Electron. Lett.*, Vol. 42, No. 3, 135–136, February 2006.
4. Barbarino, S. and F. Consoli, "Effect of the substrate permittivity on the features of a planar slot antenna," *Microw. Opt. Technol. Lett.*, Vol. 52, No. 4, 935–940, April 2010.
5. Yeo, J., "Wideband circular slot antenna with tri-band rejection characteristics at 2.45/5.45/8 GHz," *Microw. Opt. Technol. Lett.*, Vol. 50, No. 7, 1910–1914, July 2008.
6. Yang, Z., L. Li, and H. Wang, "Investigation on ultra-wideband printed circular monopole antenna with frequency-notched," *IEEE International Conference on Microwave and Millimeter Wave Technology*, Vol. 4, 1858–1861, 2008.
7. Khan, S. N., J. Xiong, and S. He, "Low profile and small size frequency notched planar monopole antenna from 3.5 to 23.64 GHz," *Microw. Opt. Technol. Lett.*, Vol. 50, No. 1, 235–236, January 2008.
8. Neyestanak, A. A. L. and A. A. Kalteh, "Band-notched elliptical slot UWB microstrip antenna with elliptical stub filled by the H-shaped slot," *Journal of Electromagnetic Waves and Applications*, Vol. 22, No. 14–15, 1993–2002, 2008.
9. Balanis, C. A., *Antenna Theory: Analysis and Design*, 2nd edition, John Wiley and Sons, New York, 1997.

10. Consoli, F., F. Maimone, and S. Barbarino, "Study of a CPW-fed circular slot antenna for UWB communications," *Microw. Opt. Technol. Lett.*, Vol. 48, No. 11, 2272–2277, Nov. 2006.
11. Chen, Z. N., *Antennas for Portable Devices*, John Wiley and Sons, Chichester, 2007.
12. Jiang, J.-B., Z.-H. Zhang, Y. Song, and W. Wu, "Band-notched UWB printed antenna with an inverted C-slotted ground," *Journal of Electromagnetic Waves and Applications*, Vol. 22, No. 14–15, 2015–2022, 2008.
13. Song, Y., Y. C. Jiao, T. L. Zhang, J. B. Jang, X. Zhang, and F. S. Zhang, "Frequency notched UWB slot antenna with a fractal-shaped slot," *Journal of Electromagnetic Waves and Applications*, Vol. 23, No. 2–3, 321–327, 2009.
14. Liu, R.-H., Z.-H. Yan, J.-B. Jang, and Y. Bai, "Small printed ultra-wideband antenna with an inverted F-slotted ground," *Journal of Electromagnetic Waves and Applications*, Vol. 23, No. 11–12, 1497–1504, 2009.
15. Movahedinia, R. and M. N. Azarmanesh, "A novel planar UWB monopole antenna with variable frequency band-notch function based on etched slot-type elc on the patch," *Microw. Opt. Technol. Lett.*, Vol. 52, No. 1, 229–232, January 2010.
16. Lamensdorfr, D. and L. Susmad, "Baseband-pulse-antenna techniques," *IEEE Antennas Propag. Mag.*, Vol. 36, No. 1, 20–30, Feb. 1994.